Thermomechanical modelling and force analysis of friction stir welding by the finite element method

C Chen and R Kovacevic

Proceedings of the Institution of Mechanical Engineers, Part C: Journal of Mechanical Engineering Science 2004 218: 509
DOI: 10.1243/095440604323052292

Thermomechanical modelling and force analysis of friction stir welding by the finite element method

C Chen and **R Kovacevic***
Research Center for Advanced Manufacturing, Department of Mechanical Engineering, Southern Methodist University, Richardson, Texas, USA

Abstract: Friction stir welding (FSW) is a solid-state jointing technology, in which the butted plates are heated, plasticized and jointed locally by the plunged probe and shoulder moving along the joint line. The residual stresses due to the thermomechanical performance of the material and the constraint of the welded plates by the fixture are one of main concerns for this process. A prediction of the clamping force applied on the plates during FSW is expected to be helpful in controlling the residual stresses and weld quality. Furthermore, the prediction of the force history in FSW will be beneficial to understand the mechanics of the process and to provide valid models for controlling the process, especially in the case of robotic FSW. In this paper, a three-dimensional model based on a finite element method is proposed to study the thermal history and stress distribution in the weld and, subsequently, to compute mechanical forces in the longitudinal, lateral and vertical directions. The proposed model includes a coupled thermomechanical modelling. The parametric investigation of the effects of the tool rotational and longitudinal speed on the longitudinal, lateral and vertical forces is also conducted in order to compute the appropriate clamping force applied on the plates. Measurements by the load cells in the longitudinal, lateral and vertical directions are presented and reveal a reasonable agreement between the experimental results and the numerical calculations.

Keywords: friction stir welding, finite element method, thermomechanical modelling, temperature history, stress distribution, mechanical forces

NOTATION

$[B]$	strain function matrix
c	heat capacity (kJ/kg °C)
$[D]$	displacement function matrix
f_x	longitudinal nodal force (N)
f_y	vertical nodal force (N)
f_z	lateral nodal force (N)
F	volume force intensity (N/m^3)
F_x	absolute value of the longitudinal force (kN)
F_y	absolute value of the vertical force (kN)
F_z	absolute value of the lateral force (kN)
k	conductivity (W/m °C)
$[M]$	stress function matrix
$p(T)$	pressure on the shoulder of the tool (N/m^2)
q	heat generation rate per unit volume (J/m^3 s)
$\dot{q}$	heat generation rate (J/s)
r	radius (m)
r_0	outer radius of the probe (m)
R_0	outer radius of the shoulder (m)
S	stress tensor (MPa)
T	temperature (°C)
ΔT	difference between the current temperature and the reference temperature (°C)
U	displacement (m)
U_y	normal displacement (m)
V	tool transverse speed (m/s)
γ	acceleration (m/s^2)
ε	total strain tensor
ε^e	elastic strain
ε^p	plastic strain
ε^t	thermal strain
$\mu(T)$	friction coefficient
ρ	material density (kg/m^3)
ω	rotational speed of the shoulder (round/s)
Ω	volume of material

The MS was received on 14 February 2003 and was accepted after revision for publication on 9 February 2004.
* *Corresponding author: Research Center for Advanced Manufacturing, Department of Mechanical Engineering, Southern Methodist University, 1500 International Parkway, Suite 100, Richardson, TX 75081, USA.*

1 INTRODUCTION

Friction stir welding (FSW) is a relatively novel technique for joining aluminium alloys [1]. In comparison with other welding techniques, FSW offers benefits for low residual stresses, low distortion and high joint strength due to the pure solid-state joining of aluminium alloys. As the welded plates are fixed in this process, the rotational and longitudinal movement of the tool will exert non-linear forces in three directions to the fixture, the welded plates and the tool itself. These forces combined with the thermal impact effect may induce the deformation of the fixture and the welded plates and affect the wear of the tool. These effects will subsequently complicate the formation of the residual stresses in the weld and the prediction of tool life. It is natural to think that the force control technology for the FSW is important and can impact the economics of welding operations through productivity and weld quality. A similar methodology has been adopted in the prediction of cutting forces [2] and their controls [3, 4]. Maintaining forces in FSW at a specific level will bring significant benefits: tool breakage prevention, tool life prediction, prediction of clamping forces, optimization design of fixture, etc.

In order to build an efficient control methodology for FSW, especially in robotic FSW, a valid force prediction model needs to be established, and many basic mechanics of this process need to be understood. It is known that the clamping force contains static non-linearities with respect to the tool rotational speed, longitudinal speed, tool plunge depth and the thermo-mechanical performance of the materials. The prediction of the mechanical force by numerical simulation will provide an insight into the correlation of the welding parameters and the weld quality and help to understand the mechanics of welding.

For FSW, much of the previous work has been concentrated on the microstructure issues and mechanical properties [5–7] of the weld. To the present authors' knowledge, sparse work has been carried out on modelling the thermomechanical performance of FSW and prediction of mechanical forces. Deng and co-workers [8, 9] used a solid-mechanics-based finite element model to simulate the plastic flow process in FSW. Several models for the modelling of thermomechanical stresses in FSW were proposed by Chao and Qi [10] and Dong *et al.* [11]. The Chao–Qi model predicted the thermal history, and the subsequent thermal stress and distortion of the work piece without involving the mechanical effect of the tool. The Dong *et al.* model took into account both friction heating and plastic work in modelling the heat flow phenomena in the FSW process and predicted the development of a plastic strain around the weld zone in the initial stage of welding. However, no longitudinal movement of the tool is involved in the Dong *et al.* simplified model for the thermomechanical process. To the present authors' knowledge, no one has predicted the mechanical forces in FSW.

In this paper, a three-dimensional model based on a finite element method (FEM) is proposed to study the thermal history and stress distribution in the weld by considering the mechanical effect of the tool (only the shoulder is included at this time). Subsequently, a study of the longitudinal, vertical and lateral force in the welding of aluminium alloy 6061 is presented. This study is accomplished by parametrically studying the effects of varying the welding parameters, primarily the rotational speed and traverse speed of the tool. The entire welding process is simulated using the commercial finite element package ANSYS. Experiments on the welding of aluminium alloy 6061-T6 are also carried out, and the temperature history and three component forces for the plates are measured for the comparison with the calculated results.

2 MODEL DESCRIPTION

The welding process is shown in Fig.1, where V is the traverse speed of the tool and ω is the rotational speed of the tool. The tool is made of AISI A2 steel and consists of the shoulder and the probe, with diameters of $R_0 = 24\,\text{mm}$ and $r_0 = 6\,\text{mm}$ respectively. The welded plates are aluminium alloy 6061-T6 in a rectangular shape with dimensions of $200\,\text{mm} \times 50\,\text{mm} \times 6.4\,\text{mm}$. The tool is considered a rigid solid, and the workpiece is considered a ductile material with elasticity, plasticity and the kinetic hardening effect. The temperature-dependent properties of aluminium alloy 6061-T6 from references [10] and [12] and the properties of AISI A2 steel [13] are listed in Table 1.

2.1 Heat transfer model

The temperature calculation is based on Fourier's equation

$$\rho\, c \frac{\mathrm{d}T}{\mathrm{d}t} = \mathrm{div}(k\ \mathrm{grad}\ T) + q \ \text{in}\ \Omega \tag{1}$$

where q is the heat generated by friction at the tool–material contact surface, Ω is a volume of the material, T is the temperature, k is the conductivity, ρ is the material density and c is the heat capacity.

The main heat source in FSW is generally considered to be the friction between the rotating tool and the welded plates, and the 'cold work' in the plastic deformation of material in the vicinity of the tool. Considering an element at the contact surface between the tool shoulder and the top surface of work piece, the

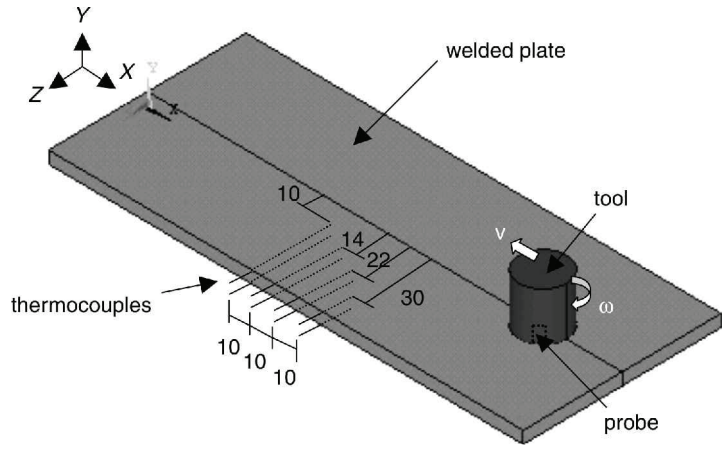

Fig. 1 A schematic illustration of FSW and arrangement of thermocouples

rate of heat generation derived from the friction in the element at radius r is

$$d\dot{q} = 2\pi\omega r^2 \mu(T)p(T)\, dr \tag{2}$$

where ω is the rotational speed of the tool, $\mu(T)$ is the coefficient of friction between the tool and the material, and $p(T)$ is the pressure on the shoulder of the tool.

The rate of heat generation (caused by the friction) over the entire interface of the contact will be

$$\dot{q} = \int_{r_0}^{R_0} 2\pi\omega r^2 \mu(T)p(T)\, dr = \frac{2}{3}\pi\omega\mu(T)p(T)\left(R_0^3 - r_0^3\right) \tag{3}$$

where R_0 and r_0 are the outer radii of the tool and the probe respectively. The rate of heat generation at the interface between the shoulder and the top of work piece surface is a function of the friction coefficient $\mu(T)$, angular velocity ω and radius r. As $\mu(T)$ and $p(T)$ are dependent on the local temperature and the radius r, equation (2) is difficult to evaluate. In this model, a constant value of the friction coefficient is used to approximate the comprehensive heat effect of friction and plastic deformation during FSW. The heat generation in the vicinity of the probe is considered to be the same as that at the shoulder periphery with a radius equal to the radius of the probe.

2.2 Mechanical model

The force equilibrium on an arbitrary volume results in the following governing equation known as the equilibrium equation:

$$\mathrm{div}(S) + F = \rho\gamma \tag{4}$$

where S is the stress tensor, ρ is the material density, γ is the acceleration and F is the volume force intensity. The inertial effect is neglected $(\gamma = 0)$ in this model since a constant rotational speed and a constant longitudinal speed are used during FSW.

The stress formed in the weldment is caused by the thermal gradient, elastic deformation and plastic deformation of the material. The stress–strain equation is described as

$$S = [M]\varepsilon \tag{5}$$

where ε is the total strain tensor and $[M]$ is the stress function matrix. The total strain tensor ε can be

Table 1 Material properties of AISI A2 steel [**8**, **10**] and aluminium alloy 6061-T6 [**11**]

	Temperature (°C)	Thermal conductivity (W/m °C)	Heat capacity (J/kg °C)	Density (kg/m^3)	Young's modulus (GPa)	Yield strength (MPa)	Thermal expansion (μm/ °C)	Poisson's ratio	Melting point (°C)
AISI A2 Steel		23.8	1096	7860	203		10.6	0.23	
Al alloy 6061-T6	0	162	917	2703	69.7	277.7	22.4		
	93.3	177	978	2685	66.2	264.6	24.61		
	204.4	192	1028	2657	59.2	218.6	26.6	0.23	582–652
	315.6	207	1078	2630	47.78	66.2	27.6		
	427.7	223	1133	2602	31.72	17.9	29.6		
	571.1	253	1230	2574	0	0	34.2		

decomposed in the following way:

$$\varepsilon = \varepsilon^{e} + \varepsilon^{p} + \varepsilon^{t} \tag{6}$$

where ε^{e} is the elastic part, ε^{p} is the plastic part and ε^{t} is the thermal part.

Thermal strain can be computed by

$$\varepsilon^{t} = [B]\ \Delta T \tag{7}$$

where $[B]$ is the strain function matrix and ΔT is the difference between the current temperature and the reference temperature.

Displacement is given by

$$U = [D]\varepsilon \tag{8}$$

where $[D]$ is the displacement function matrix. In the displacement formulation, the essential boundary conditions are specified as

$$U = 0 \tag{9}$$

for the clamped portion of the plate surface and the normal displacement

$$U_y = 0 \tag{10}$$

for the bottom of the plate at $y = 0$.

2.3 Finite element model

ANSYS as a commercial FEM software is used to carry out the numerical simulation. In the simulation, the thermomechanically coupled three-dimensional Lagrangian finite element model incorporating temperature and multilinear strain hardening effects is used for the three-dimensional modelling of the solid structures. Temperature-dependent properties of aluminium alloy 6061 are used in the modelling. The element topology used is eight nodes having three degrees of freedom at each node: translations in the nodal x, y and z directions [**14**]. The element has plasticity, stress stiffening, large deflection and large strain capabilities [**14**].

Symmetry along the weld line is assumed in this preliminary calculation in order to save computation time; therefore, one half of the welded plate (at the retreating side) is meshed as shown in Fig. 2, with a total of 3537 nodes. In modelling the temperature history, the moving heat sources of the shoulder and the probe are represented as moving the heat generation of the nodes in each computational time step. The Coulomb friction law is applied for the interaction between the shoulder and the material. The relatively larger contact region of the shoulder material compared with that of the probe material is assumed to contribute most of the force formed in this process. It should be noted that the rotation of the tool will produce not exactly symmetrical stress results in the plates on the advancing side and the retreating side during the welding. However, considering that the stress in the plates is mostly from the friction-derived thermal effect rather than from the mechanical action of the tool (confirmed by our preliminary calculations of stress without involving the thermal effect), it should be reasonable to expect that Fig. 6 (shown later) can well reflect the stress distribution of the welded plates on the retreating side during the welding.

As the temperature gradient is large around the welding zone, seriously changes the materials properties and subsequently affects the mechanical solution, the thermal and mechanical solutions are coupled; the temperature datum at each increment time is used to evaluate the mechanical and thermal properties.

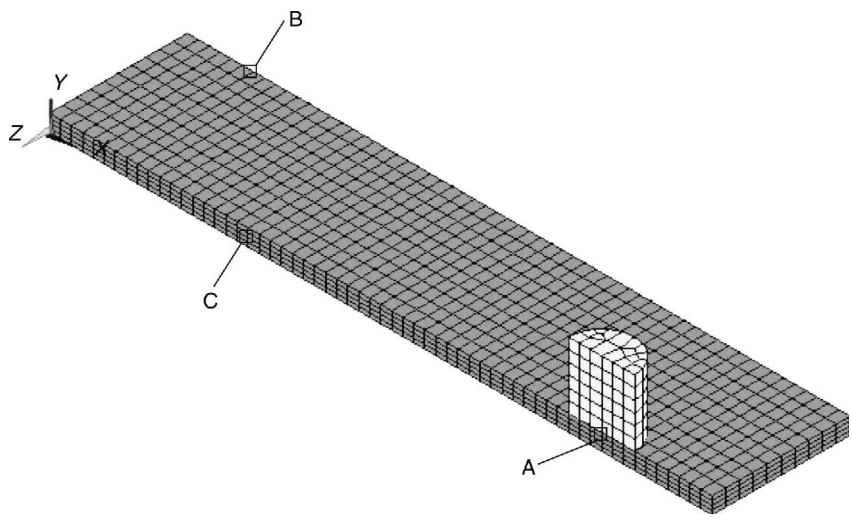

Fig. 2 Finite element model for the welded plate and the tool; node A is located on the tool side, and nodes B and C correspond to the locations of the two load cells, respectively

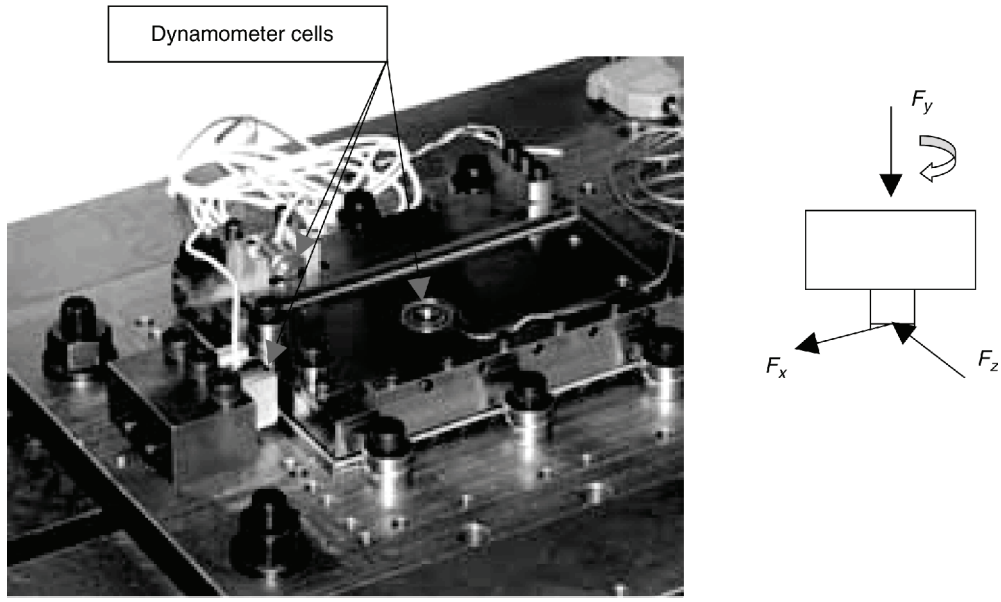

Fig. 3 Three-axis force measurement device

3 EXPERIMENT SET-UP

A heavy-duty vertical milling machine is adapted for the FSW experiments. Appropriate fixturing and tooling have been developed in house. A sensor based on a micrometer measuring unit is used to monitor the plunge depth of the tool. In the experiments, eight thermal couples are embedded in one plate with four located 1.6 mm below the top surface and four located 1.6 mm from the bottom surface, with a distance of 10 mm, 14 mm, 22 mm and 30 mm respectively to the weld centre-line (see Fig. 1). The spacing of the thermocouples in the longitudinal direction is 10 mm. A three-axis force measurement system composed of three load cells with a range of 1–10 000 lb has been developed, as shown in Fig. 3. Temperatures and three orthogonal force components are acquired and recorded in a time duration of 0.1 s by a Labview-programmed acquisition system [**15**].

4 DISCUSSION OF NUMERICALLY SIMULATED AND EXPERIMENTAL RESULTS

4.1 Study of thermal history in FSW

Figure 4 shows a comparison of the calculated and the measured temperature histories at the location 10 mm to the weld centre-line and 1.6 mm below the top surface. The rotational speed and the traverse speed of the tool are 500 r/min and 140 mm/min respectively. In the initial stage of the welding, the calculated values are higher

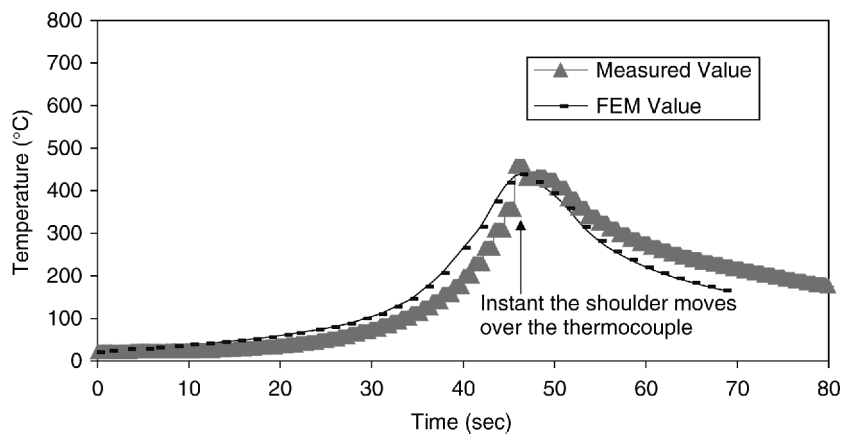

Fig. 4 A comparison of the calculated and the measured temperature histories at the location 10 mm to the weld centre-line and 1.6 mm below the top surface of the plate ($V = 140$ mm/min and $\omega = 500$ r/min)

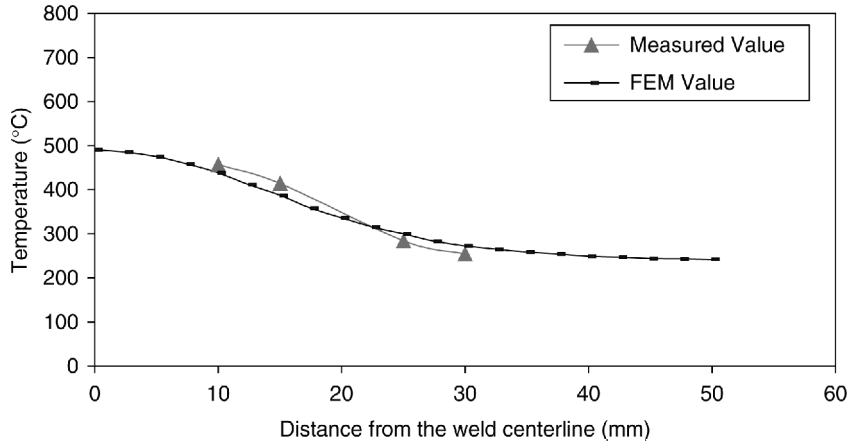

Fig. 5 A comparison of predicted temperature distribution and measurement along the lateral direction for nodes 1.6 mm below the top surface of the plate ($V = 140$ mm/min, $\omega = 500$ r/min and $t = 34$ s)

than the measured values, but they are lower than the measured values after the maximum temperature is reached, which may be caused by the assumption of a constant temperature of the backing plate. In fact, the temperature of the backing plate rises because of the heat build-up during welding, which decreases the cooling rate of the weld. Nevertheless, the calculated temperature values in the whole welding process are in reasonable agreement with the measured values. Figure 5 shows a temperature distribution along the lateral direction (for nodes 1.6 mm below the top surface of the plate) at the instant the shoulder's centre passes over this location. Good agreement between the measured and calculated temperatures indicates that the developed model for the prediction of temperature history is providing valuable results.

4.2 Analysis of stress distribution in the weld

Stress will form in the weld during welding since expansion of the material occurs during heating of the welded plates, followed by contraction during cooling of the welds. Furthermore, a mechanical reaction effect in the weld zone due to the rotational movement and the transverse movement of the tool will cause additional stress in the weld.

Figure 6 shows the stress distribution in the welded plate at the retreating side and the tool in three directions at the time of 34 s (step 20) after the start of the welding. Figure 6a shows the principal stress distribution in the longitudinal direction (X direction). It can be seen that most of the region (A and B) in the plate in front of the tool is subjected to a compressive stress (minus value), with a minimum value on the back side of the plate indicated by MN. The regions of C, D and E in the plate behind the tool are subjected to a tensile stress with a maximum value on the back side of the plate indicated by MX. The stress distribution on the shoulder top surface is relatively uniform.

In the vertical direction (Y direction), most of the regions (A, B and C) in the plate except for region D are subjected to compressive stress, as shown in Fig. 6b. The minimum and maximum stress values for the plate are indicated by MN and MX respectively. The reason for the locations of the minimum and maximum stress values can be explained by the combination of the thermal effect, clamping of the plate and mechanical effect of the shoulder. The modelling of the stress distribution in FSW without considering the thermal effect has been carried out, and the computed results show that the minimum stress in the plate is formed in the region beneath the tool with a maximum intensity formed in the region around the tool.

Figure 6c shows the stress distribution in the welded plate and the tool along the lateral direction (Z direction). The compressive stress forms in the regions A and B in the front part of the plate and tensile stress forms in the regions C, D and E behind the tool. The minimum and maximum stress values formed in the plate are located in the front end point and rear end point of the plate respectively, with the furthest distances from the tool denoted by MN and MX respectively.

4.3 Parametric study of three-axis force components

Based on the simulated stress results described above, the mechanical force in the longitudinal direction (X direction) is computed by integrating the stresses at the nodes of the shoulder in contact with the plate. The mechanical forces in the lateral and vertical directions are computed by integrating the stresses at the nodes in contact with the dynamometer cells. The mechanical force history formed during FSW at various rotational

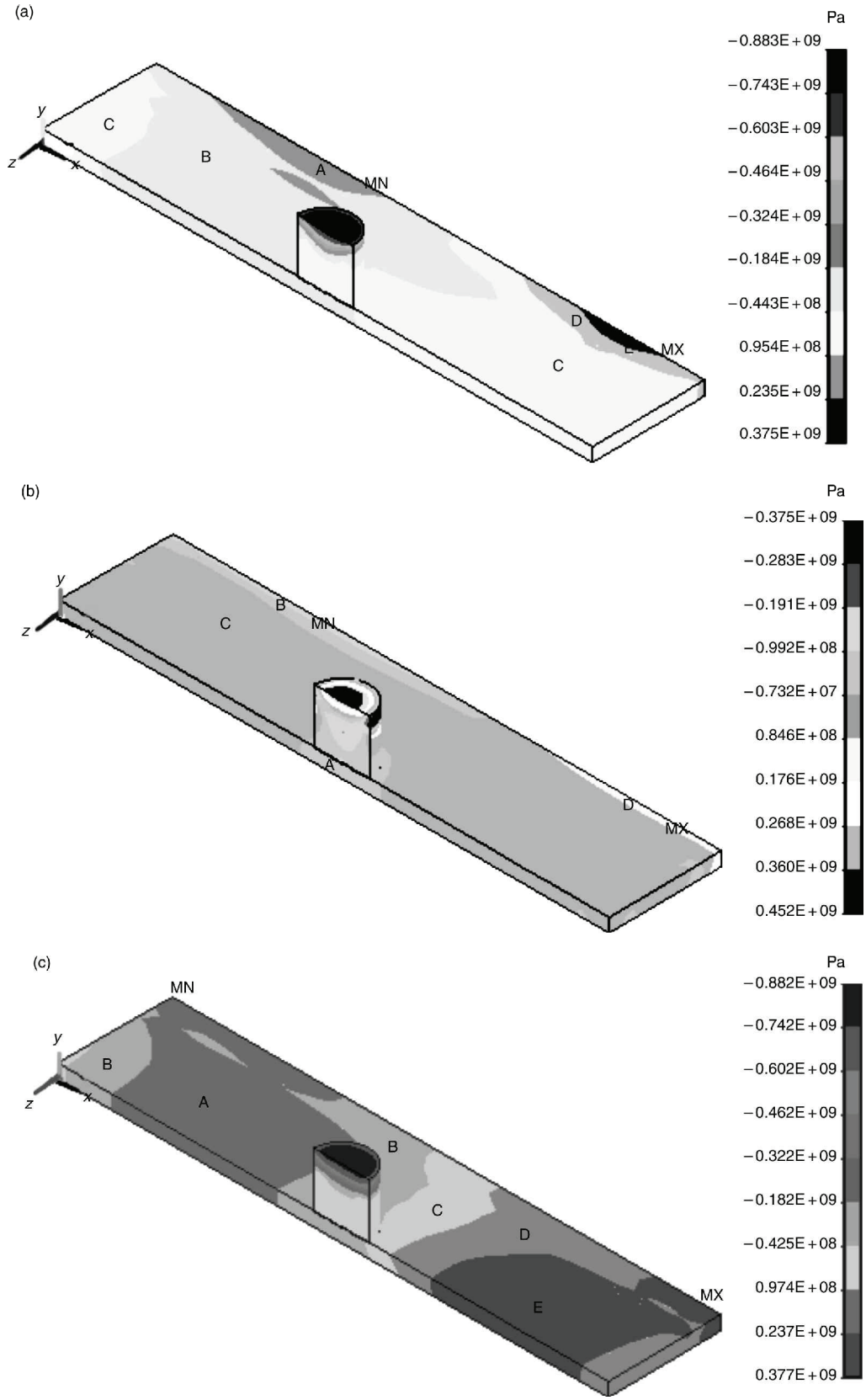

Fig. 6 Predicted principal stress distributions in the welded plate and the tool in three directions at a time of 34 s (step 20) after the start of welding: (a) x direction; (b) y direction; (c) z direction

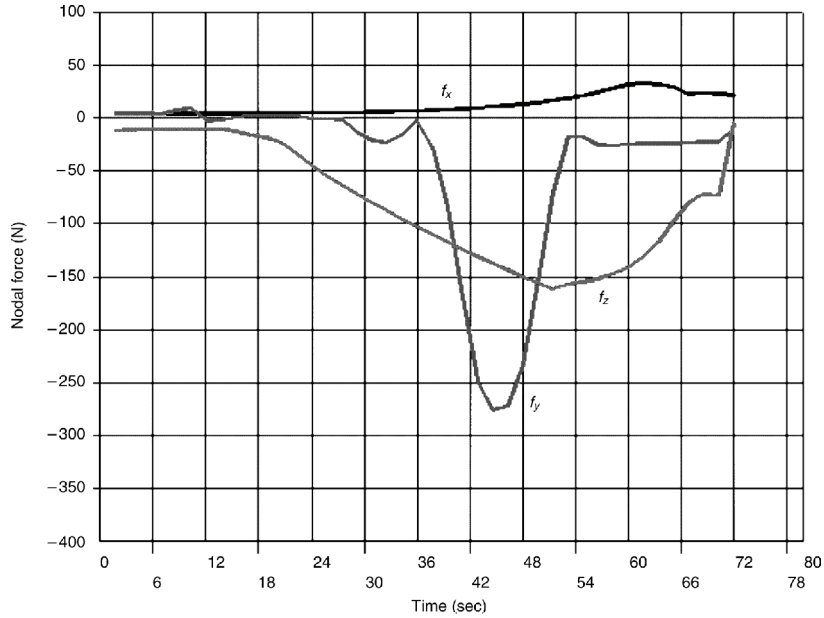

Fig. 7 Predicted nodal force histories for nodes A, B and C indicated in Fig. 2

and traverse speeds of the tool are simulated, and some of the obtained results follow.

4.3.1 *Analysis of effects of rotational speed on force components*

The effects of the variation in the rotational speed of the tool on the mechanical forces are studied by setting the traverse speed at 140 mm/min, and the rotational speeds of the tool are varied from 344 to 757 r/min. Figure 7 shows the predicted nodal force history for nodes A, B and C indicated in Fig. 2. Based on all the predicted nodal forces, the force histories in three directions are obtained as shown in Fig. 8, from which it is seen that the force in the longitudinal direction reveals an increasing trend as the rotational speed is increased. The maximum force values in the vertical and lateral directions match the instant that the tool moves over the corresponding sensors. The maximum force value in the vertical direction increases with increasing rotational speed of the tool in the range 344–757 r/min, with a slight increase in the lateral direction on increasing the rotational speed. From the simulated results, it is revealed that the mechanical forces in the longitudinal and vertical directions can be reduced by increasing the rotational speed of the tool in a certain range, while the lateral force is weakly linked with the rotational speed of the tool. It is noted that the predicted force values show fluctuation due to the discretization involved in plate meshing and step movement in the FEM simulations, especially for the force in the longitudinal direction.

4.3.2 *Analysis of effect of traverse speed on force components*

The traverse speed is an important parameter that is directly related to the production efficiency. A study of the effect of the traverse speed on the longitudinal, vertical and lateral forces is carried out by setting the rotational speed of the tool to 500 r/min. For convenience in analysis, the maximum force values in the vertical and lateral directions and the average force value in the longitudinal direction are used for the analysis.

Figure 9 shows the force values for various rotational speeds of the tool, and it is obvious that the forces in the longitudinal and lateral directions increase with increasing traverse speed. A slight increase in the mechanical force in the vertical direction occurs with increasing traverse speed. This increase means that the traverse speed will mainly affect the lateral and longitudinal forces, with little effect on the vertical force.

5 EXPERIMENTAL WORK AND VALIDATION OF THE MECHANICAL FORCE MODEL

Figure 10 shows a comparison of the predicted force values and the measurements in three directions at a rotational speed of 500 r/min and a traverse speed of 140 mm/min. The predicted force values show fluctuation, especially for the force in the longitudinal direction. The fluctuation in the predicted force values is due to the discretization involved in plate meshing and step movement in FEM simulation. A serious fluctua-

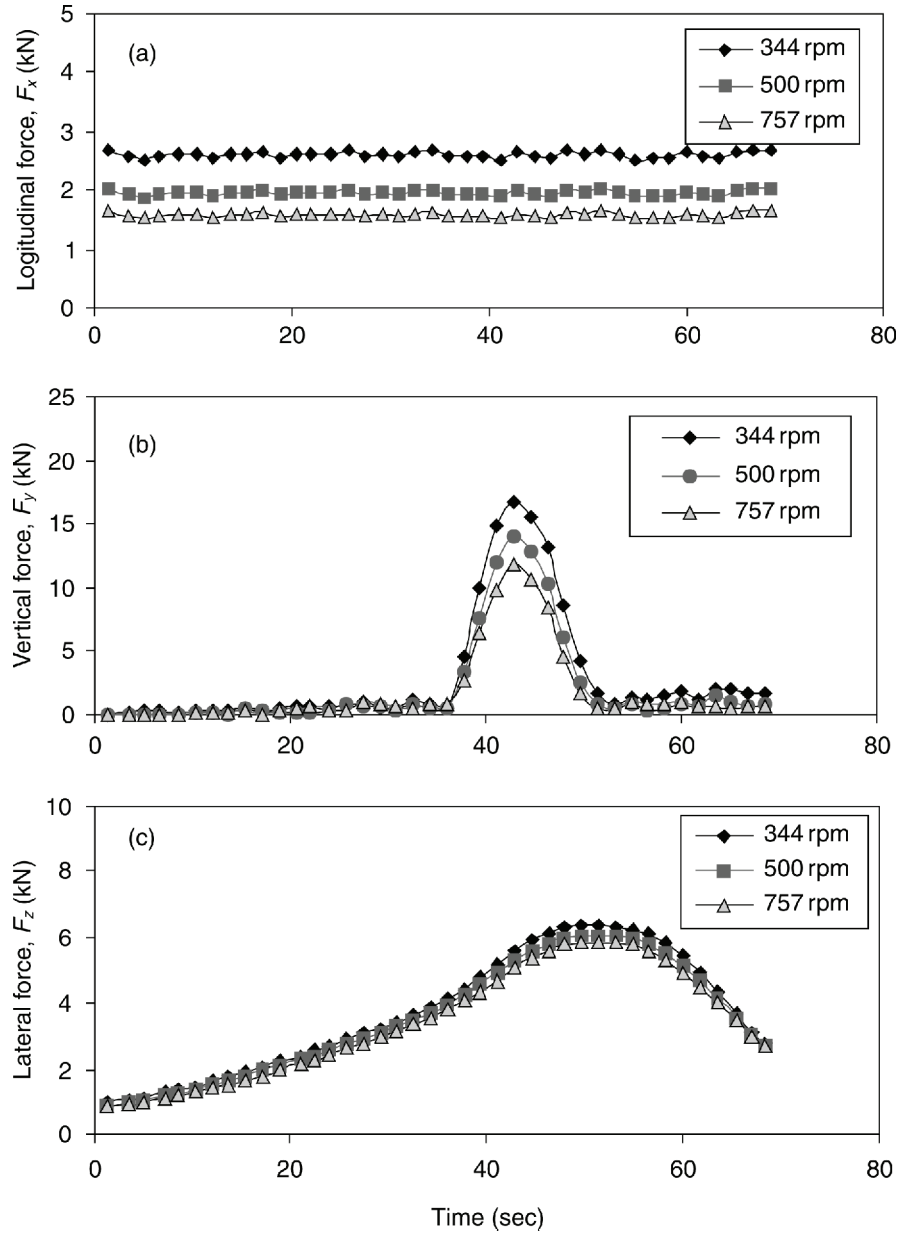

Fig. 8 Predicted mechanical force histories in three directions (as indicated in Fig. 4) at various rotational speeds of the tool: (a) 344 r/min; (b) 500 r/min; (c) 757 r/min (under constant $V = 140$ mm/min)

tion in force happens in the longitudinal direction for both the predicted values and the measured values, as shown in Fig. 10a. The fluctuation in force measurements in the longitudinal direction is due to the discrete linear movement of the table and flash formation in the plate during the welding. It is noted that there are small fluctuations in the forces in the lateral and vertical directions, as shown in Figs 10b and c.

Figure 10a also reveals that the measured vertical force F_y increases as the tool travels along the welding direction, which is caused by the offset of the plate portion ahead of the tool in the Y direction as a dynamometer set-up requirement. It is expected that the offset in three directions, the dynamometer set-up requirement, may contribute in main part to the discrepancy between the force predictions and measurements. However, the predicted force values are in a reasonable agreement with the measurements, which validates the efficiency of the force simulation model.

6 CONCLUSIONS

A three-dimensional thermomechanical model of the FSW of an aluminium alloy is developed in order to

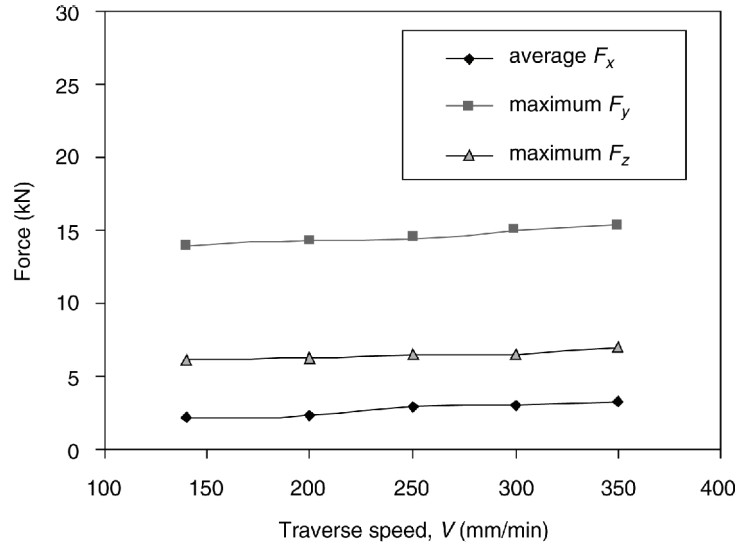

Fig. 9 Predicted mechanical forces in three directions as indicated in Fig. 4 at various traverse speeds of the tool ($\omega = 500\,\mathrm{r/min}$)

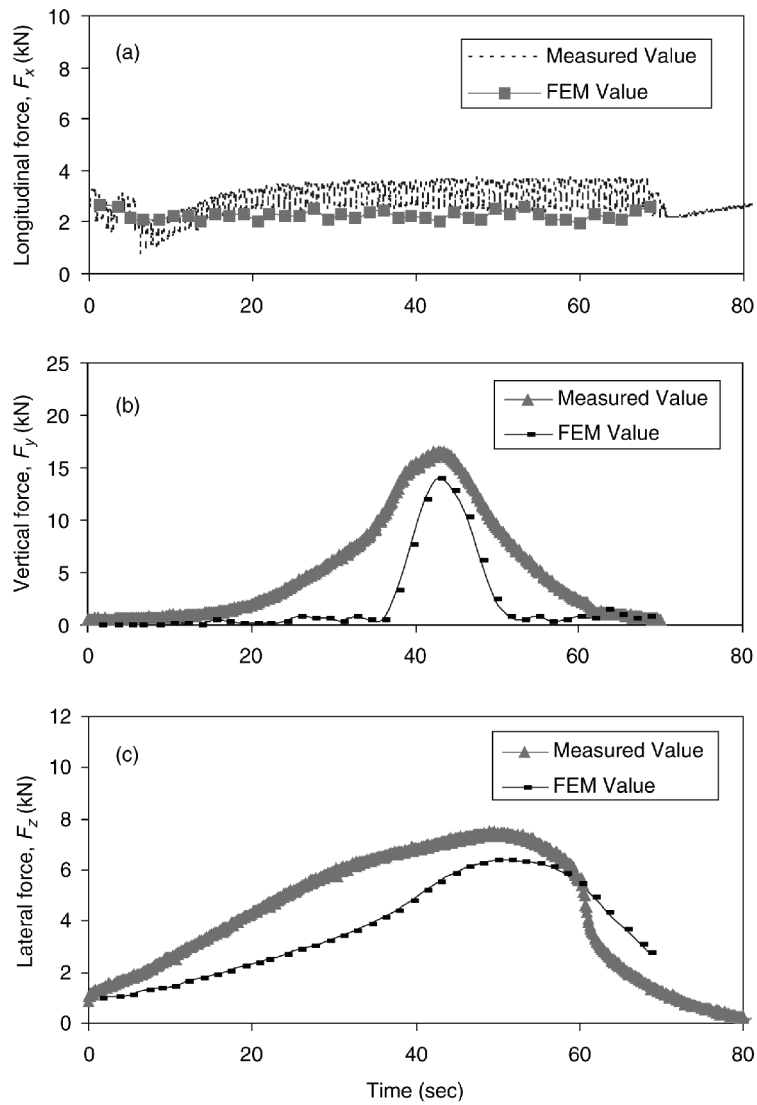

Fig. 10 Comparison of predicted and measured mechanical force histories in three directions as indicated in Fig. 4 ($\omega = 500\,\mathrm{r/min}$ and $V = 140$ mm/min): (a) F_x; (b) F_y; (c) F_z

understand the stress evolution in the welding. The resulting stress data are subsequently used to predict the three axial force components exerted on the plate. Parametric studies have been carried out to determine the effect of the rotational speed, the traverse speed on the stress distribution, and the mechanical force. A comparison of the simulated results and the measured data for both the temperature and the force shows reasonable agreement. The prediction shows that the longitudinal force is strongly influenced by the welding parameters. It decreases with increase in the tool rotational speed and increases with increasing traverse speed. A strong fluctuation in force occurs in the longitudinal direction. The vertical force decreases with increase in the rotational speed and increases slightly with increase in the traverse speed. The lateral force has a weak link with the rotational speed and increases slightly with increase in the traverse speed. The simulated results are expected to be helpful in optimizing the welding process to ensure good weld quality and in facilitating the automation of the process.

ACKNOWLEDGEMENTS

The authors are grateful for the financial support of the US Department of Education (Grant P200A80806-98) and the American Welding Society and also thank Mr Michael Valant for technical assistance in preparing the experiments.

REFERENCES

1 **Thomas, W. M., Nicholas, E. D., Needham, J. C., Murch, M. G., Templesmith, P.** and **Dawes, C. J.** Friction stir butt welding. Int. Pat. Applic. PCT/GB92/02203, GB Pat. Applic. 9125978.8, 6 December 1991.

2 **Kumbera, T. G., Cherukuri, H. P., Patten, J. A., Brand, C. J.** and **Marusich, T. D.** Numerical simulations of ductile machining of silicon nitride with a cutting tool for defined geometry. *J. Machining Sci. Technol.*, 2001, **5**(3), 341–352.

3 **Landers, R. G.** and **Lu, Y. W.** Stability analysis of nonliear machining force controllers. In Proceedings of the American Control Conference, San Diego, California, 2–4 June 1999, pp. 679–683.

4 **Shimizu, K., Matsuoka, S.-I., Yamazaki, N.** and **Oki, Y.** High-speed cutting for extruded aluminum alloys using robot. *J. Japan Inst. Light Metals*, 1998, **48**(12), 603–607.

5 **Reynolds, A. P., Lockwood, W. D.** and **Seidel, T. U.** Processing–property correlation in friction stir welds. *Mater. Sci. Forum*, 2000, **331–337**, 1719–1724.

6 **Murr, L. E., Li, Y., Trillo, E. A.** and **McClure, J. C.** Fundamental issues and industrial applications of friction-stir welding. *Mater. Technol.*, 2000, **15**(1), 37–48.

7 **Dawes, C. J.** and **Thomas, W. M.** Friction stir process for aluminum alloys. *Weld. J.*, 1996, **75**(3), 41–45.

8 **Deng, X.** and **Xu, S.** Solid mechanics simulation of friction stir welding process, *Trans. NAMR–SME*, 2001, **29**, 631–638.

9 **Xu, S., Deng, X., Raynolds, A. P.** and **Seidel, T. U.** Finite element simulation of material flow in friction stir welding. *Sci. Technol. Weld. Joining*, 2001, **6**(3), 191–193.

10 **Chao, Y.** and **Qi, X.** Thermal and thermo-mechanical modeling of friction stir welding of aluminum alloy 6001-T6. *J. Mater. Processing Mfg Sci.*, 1998, **7**(10), 215–233.

11 **Dong, P., Lu, F., Hong, J. K.** and **Cao, Z.** Coupled thermomechanical analysis of friction stir welding process using simplified models. *Sci. Technol. Weld. Joining*, 2001, **6**(5), 281–287.

12 *Handbook of Aluminum*, 1970 (Alcan Aluminum Corporation).

13 www.matweb.com.

14 *ANSYS User's Manual, Elements*, Release 5.7, Vol. III (Swanson Analysis Systems, Inc.).

15 www.ni.com.